

Molecular dynamics study of charged dendrimers in salt-free solution: Effect of counterions

Andrey A. Gurtovenko^{a)}

Institute of Macromolecular Compounds, Russian Academy of Sciences, Bolshoi Prospect 31, V.O., St. Petersburg 199004, Russia, and Laboratory of Physics and Helsinki Institute of Physics, Helsinki University of Technology, P.O. Box 1100, FIN-02015 HUT, Finland

Sergey V. Lyulin

Institute of Macromolecular Compounds, Russian Academy of Sciences, Bolshoi Prospect 31, V.O., St. Petersburg 199004, Russia

Mikko Karttunen

Biophysics and Statistical Mechanics Group, Laboratory of Computational Engineering, Helsinki University of Technology, P.O. Box 9203, FIN-02015 HUT, Finland, and Department of Applied Mathematics, University of Western Ontario, 1151 Richmond Street North, London (Ontario) N6A 5B7, Canada

Ilpo Vattulainen

Laboratory of Physics and Helsinki Institute of Physics, Helsinki University of Technology, P.O. Box 1100, FIN-02015 HUT, Finland; Memphys-Center for Biomembrane Physics, Physics Department, University of Southern Denmark, Campusvej 55, DK-5230 Odense M, Denmark; and Institute of Physics, Tampere University of Technology, P.O. Box 692, FIN-33101 Tampere, Finland

(Received 8 November 2005; accepted 19 December 2005; published online 7 March 2006)

Polyamidoamine dendrimers, being protonated under physiological conditions, represent a promising class of nonviral, nanosized vectors for drug and gene delivery. We performed extensive molecular dynamics simulations of a generic model dendrimer in a salt-free solution with dendrimer's terminal beads positively charged. Solvent molecules as well as counterions were explicitly included as interacting beads. We find that the size of the charged dendrimer depends *nonmonotonically* on the strength of electrostatic interactions demonstrating a maximum when the Bjerrum length equals the diameter of a bead. Many other structural and dynamic characteristics of charged dendrimers are also found to follow this pattern. We address such a behavior to the interplay between repulsive interactions of the charged terminal beads and their attractive interactions with oppositely charged counterions. The former favors swelling at small Bjerrum lengths and the latter promotes counterion condensation. Thus, counterions can have a dramatic effect on the structure and dynamics of charged dendrimers and, under certain conditions, cannot be treated implicitly. © 2006 American Institute of Physics. [DOI: [10.1063/1.2166396](https://doi.org/10.1063/1.2166396)]

I. INTRODUCTION

Dendrimers, characterized by regular branching with radial symmetry, represent a unique class of polymers possessing a large number of functional terminal groups in their outermost dendritic shell.¹ These “dream molecules”² have recently attracted a lot of attention due to potential applications in technology and medicine, see, for example, Refs. 3–5 and references therein. Polyamidoamine (PAMAM) dendrimers, in particular, are commonly used molecules in this field. They are protonated under physiological conditions,^{3,6} thus their high surface charge coupled to their ability to adapt conformation in response to changes in their surrounding environment makes PAMAM dendrimers very attractive candidates for biomedical applications such as drug and gene delivery.^{3,7–13} Thus far, most theoretical and computational investigations have focused on neutral dendrimers.^{14,15}

Since the pioneering paper of Welch and Muthukumar,¹⁶ there have been only a few computational studies of charged

model dendrimers.^{16–19} While these studies have provided a great deal of insight into the properties of dendrimers, it is obvious that their scope has been limited due to a major computational cost associated with modeling of complex dendrimers in a hydrodynamic solvent. Hence, the previous studies have treated the groups of a charged dendrimer using the linearized Poisson–Boltzmann (Debye–Hückel) theory and the solvent as a continuous medium. Despite these limitations, the above simulations demonstrated that the strength of electrostatic interactions may have a strong effect on the dendrimer's size as well as on other structural and dynamic properties. In particular, it was shown that the size of any charged dendrimer increases for an increasing effective screening length which corresponds to a decreasing salt concentration.^{16–19}

As for more accurate treatments, Lee *et al.*²⁰ simulated PAMAM dendrimers at an atomic resolution. They found that a PAMAM dendrimer swells significantly when pH decreases from a high pH value (no amines are protonated) to neutral (all the primary amines are protonated) and to low pH (all the primary amines and tertiary amines are proto-

^{a)}Electronic mail: agu@fyslab.hut.fi

nated). However, they treated the counterions as well as the solvent implicitly (except for dendrimers of second generation which were solvated in explicit water).²⁰ A more realistic atomic-scale simulation of PAMAM dendrimers was performed very recently by Maiti *et al.*²¹ and Lin *et al.*,²² who accounted for water molecules and counterions in an explicit manner. They showed that the presence of a solvent leads to a swelling of the dendrimer, while the effect of *pH* was found to be similar to that reported in earlier studies.²⁰ As a part of counterions were found to condense onto the dendrimer,²¹ it was stated that the presence of counterions increases the swelling of a dendrimer. The effect of counterions on dendrimer charges and related structural aspects was not clarified, though, since for the counterion concentrations they used, the amine charges were strongly screened: The corresponding Debye length was about 3–4 Å and hence close to the minimal value considered by Welch and Muthukumar.¹⁶ This implies that the effect of smaller counterion concentrations and, hence, the overall role of counterions has remained unresolved.

In general, there is a reason to emphasize that the applicability of the Debye–Hückel approximation for dendrimers should not be taken for granted. It is valid in the dilute limit—here it means the situation where the separation between charges exceeds the Bjerrum length. However, that condition breaks down easily in dense structures such as dendrimers, which implies that in most of the cases counterions must be taken *explicitly* into account. Computational studies of flexible linear polyelectrolytes have demonstrated^{23–25} that the presence of explicit counterions is indeed crucial: Increasing the strength of electrostatic interactions can provoke counterion condensation and, therefore, lead to dramatic changes in the polymer's structure and dynamics. It is reasonable to expect similar counterion effects also for dendrimers. A recent computational study of model dendrimers suggests that this is indeed the case.²⁶

In this study we aim to clarify the role of counterions. We have performed extensive molecular dynamics simulations using a generic cationic model dendrimer of the fourth generation. Counterions and solvent molecules are explicitly included. A systematic variation of the strength of electrostatic interactions has allowed us to examine the influence of counterions on the structural and dynamical properties of charged dendrimers. It turns out that the size of charged dendrimers depends *nonmonotonically* on the strength of electrostatic interactions in the system clearly indicating a pronounced effect of counterion condensation.

II. MODEL AND SIMULATION DETAILS

We performed molecular-dynamic (MD) simulations of dendrimers of the fourth generation using the freely jointed “bead-and-spring” model. Each bead of the last, or the terminal, generation was set to carry a positive unit charge. The dendrimer was solvated in a box of nonpolar molecules (beads) and an appropriate number of counterions were added to preserve overall charge neutrality.

The bonds were modeled as harmonic springs with their potential energy given by $U = \frac{1}{2}k(l-l_0)^2$, where l_0 is the ref-

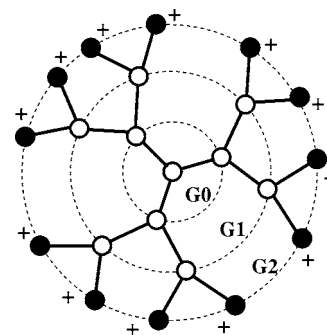


FIG. 1. A sketch of the dendritic topology used in this study. Beads of the last, or the terminal, generation shell (the illustration is for a dendrimer of the second generation) are positively charged (black beads). In the simulations we used dendrimers of the fourth generation.

erence bond length. The spring constant $k = 10^3 k_B T / l_0^2$ was chosen to be rather high as has been done in earlier studies.²⁷ All short-range nonelectrostatic nonbonded interactions were described by the Lennard-Jones potential $U_{LJ} = 4\epsilon[(\sigma/r)^{12} - (\sigma/r)^6]$ with $\epsilon = 0.3k_B T$. The bead-bead interaction diameter $\sigma = 0.8l_0$ was taken to be the same for all beads in the system. The Lennard-Jones potential was cut off at $r_c = 2^{1/6}\sigma$ and shifted to zero.²³ The dendrimer was in a good solvent.

The long-range electrostatic interactions between the charged terminal beads (with a positive unit charge on each) and negatively charged counterions were handled using the particle-mesh Ewald (PME) method,^{28,29} which has been shown to perform well in soft matter simulations.^{30,31} The strength of electrostatic interactions is characterized by the so-called Bjerrum length:

$$\lambda_B = \frac{e^2}{4\pi\epsilon_0\epsilon_s k_B T}, \quad (1)$$

where ϵ_s is the dielectric permittivity of the solvent. To examine the effects of counterions on the dendrimer's structure and dynamics, the Bjerrum length λ_B was systematically varied from 0 to $8.0l_0$. This change in λ_B may be interpreted as a variation of the dielectric properties of the solvent ($\lambda_B \sim 1/\epsilon_s$). In all, we studied ten different systems with λ_B/l_0 taken to be 0.0, 0.2, 0.4, 0.6, 0.8, 1.0, 2.0, 3.2, 6.4, and 8.0.

The dendritic topology employed in our study is schematically depicted in Fig. 1. We studied a trifunctional dendrimer of the fourth generation with single bonds between the branch points. The dendrimer had 94 beads of which 48 were terminal ones. To generate initial configurations, the procedure of Murat and Grest was used.³² The dendrimer was then solvated in a cubic box with 4692 solvent particles. That corresponds to a polymer fraction of about 0.02. The density was set to $1.688l_0^{-3}$ (or, alternatively, to $0.864\sigma^{-3}$), similar to Refs. 33 and 34. The linear size of the simulation box size was set to $14.16l_0$, and periodic boundary conditions were applied in all three dimensions. The ratio of the average dendrimer size to the simulation box size was about 0.2.

For simulating charged dendrimers, unit positive charges were assigned to all beads of the terminal G4 generation shell of the neutral dendrimer. This was aimed to mimic physiological (neutral) *pH* conditions when the primary amines of a PAMAM dendrimer become protonated.⁶ To

keep the system electroneutral, randomly chosen 48 solvent beads were converted to counterions by assigning negative unit charges on them. This system was used as the starting configuration for MD simulations of charged dendrimers.

All systems with different Bjerrum lengths were first equilibrated for 10^6 time steps in the *NVT* ensemble with the time step $\Delta t = 2.4 \times 10^{-3} \tau_0$, where $\tau_0 = l_0(m/\epsilon)^{1/2}$ is the characteristic time of the model (m is the mass of a bead). The equilibration procedure was applied to the entire system (a dendrimer, solvent molecules, and counterions). The temperature was controlled using the scheme of Berendsen *et al.*,³⁵ while all the bond lengths were kept constant by using the SHAKE algorithm.³⁶ After equilibration, data were collected from production runs of 10^7 time steps each in the *NVE* ensemble. The time step in the production runs was set to $1.2 \times 10^{-3} \tau_0$ (constraints were not applied to dendrimer's bonds during the production). All the simulations were performed using the GROMACS package.^{37,38} Each simulation was run on a single 3.2 GHz Pentium-4 processor.

To examine possible finite size effects, we performed additional simulation runs using simulations containing twice the number of solvent molecules. We examined the box size effects for a neutral dendrimer as well as for the charged dendrimers with $\lambda_B = 0.4l_0$ and $\lambda_B = 6.4l_0$. For the case of neutral dendrimers we did not find any noticeable deviations when the larger box size was employed. For charged dendrimers, the average size of the counterion cloud around the dendrimer was found to naturally increase upon increasing the box size. This was accompanied by a slight decrease of the fraction of counterions condensed onto the dendrimer with the corresponding small increase of the dendrimer size. This effect was found to become weaker for an increasing magnitude of electrostatic interactions in the system, so that it became indistinguishable for $\lambda_B = 6.4l_0$. Thus, increasing the simulation box size does not change the character of the λ_B dependence of the structural and dynamic properties of dendrimers.

III. STRUCTURAL PROPERTIES

A. Equilibration

As in previous computational studies,^{17,27} initial equilibration was monitored through the time evolution of the mean-square radius of gyration:

$$R_g^2 = \frac{1}{N} \sum_{i=1}^N (r_i - R_{c.m.})^2, \quad (2)$$

where N is the number of beads and $R_{c.m.}$ is the position of the center of mass (c.m.) of the dendrimer. This quantity, being a measure of the overall size of the dendrimer, was found to remain stable during the entire production run.

The above, however, is not enough for a system containing unscreened charges. It is further required that the ions have reached equilibrium. To monitor the equilibration of ions, we first calculated the radial distribution functions (RDFs) for ion-ion, ion-dendrimer bead, and ion-solvent molecule pairs (data not shown). The position of the first minimum defines the radius of the first coordination shell of

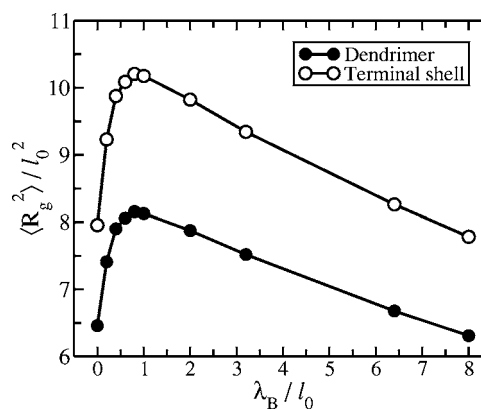


FIG. 2. Average mean-square radius of gyration $\langle R_g^2 \rangle$ of the whole dendrimer (solid circles), and of the beads of the *terminal* dendrimer shell (open circles) as a function of the Bjerrum length λ_B . Error bars are of the same size as the symbols. The error bars were estimated as the standard errors of the mean by splitting trajectories into ten pieces of 10^6 time steps each.

a counterion. This procedure has been used in other related studies as well.^{39–41} The radius was found to be $\sim 1.3l_0$. The coordination numbers were then calculated by counting the total numbers of beads within the first coordination shell. The coordination numbers are found to become stable as a function of time during the equilibration period (see Sec. II).

B. Dendrimer size and counterion condensation

Next, we describe the structural characteristics of charged dendrimers at different strengths of electrostatic interactions. In Fig. 2 we plot the average mean-square radius of gyration $\langle R_g^2 \rangle$ of the dendrimer as a function of the Bjerrum length λ_B . Remarkably, the dependence of $\langle R_g^2 \rangle$ on λ_B is found to be nonmonotonic. Increasing the Bjerrum length from zero leads to a pronounced swelling of the dendrimer, the maximum being at $\lambda_B \approx 0.8l_0$ as shown in Fig. 2. Further increase is found to have an opposite effect, i.e., the dendrimer shrinks. Figure 3 shows snapshots from our simulations for the swollen and shrunk dendrimers. Such a behavior resembles the findings for linear^{23,25} and dendritic²⁶ polyelectrolytes, and is associated with counterion condensation. In particular, a similar nonmonotonic dependence of the dendrimer size on the Bjerrum length was found in Ref. 26, where the authors considered a different dendritic topology (a dendrimer of the fifth generation with two spacers between branching points), employed a different simulation technique (Monte Carlo), and did not account for explicit solvent molecules. This suggests that as far as the structural properties are concerned, the results presented here are of generic nature. In turn, the explicit representation of solvent molecules in our case seems to lead to an overall swelling of a dendrimer compared with implicit solvent treatment and, being coupled to the molecular dynamics method employed, allows us to extract the information related to the dendrimer dynamics in an accurate manner.

The λ_B dependence for the radius of gyration calculated for charged beads of the terminal shell ($\langle R_{g,term}^2 \rangle$) follows closely that of the whole dendrimer ($\langle R_{g,dend}^2 \rangle$), see Fig. 2. Interestingly, the $\langle R_{g,term}^2 \rangle$ exceeds the radius of gyration of the dendrimer at all Bjerrum lengths. For neutral dendrimers

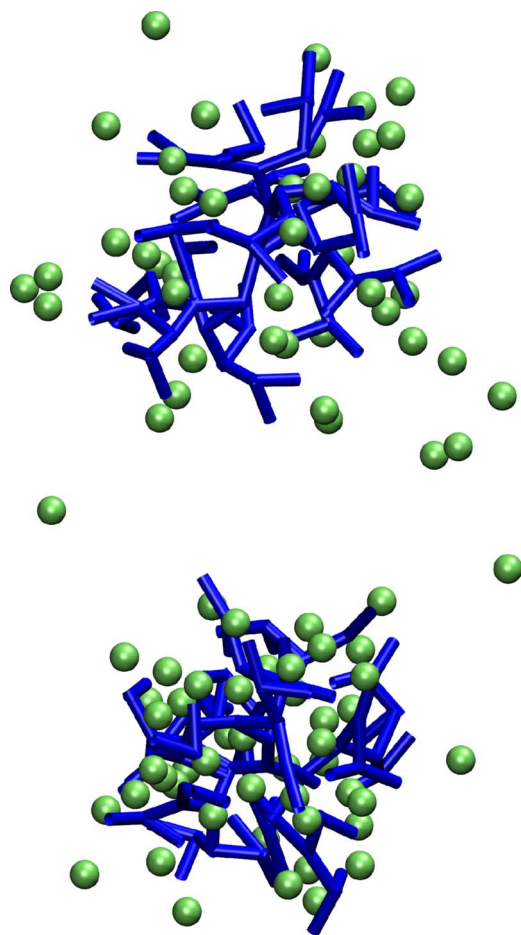


FIG. 3. (Color online) Typical configurations of charged dendrimers at $\lambda_B = 0.8l_0$ (top) and $\lambda_B = 6.4l_0$ (bottom). Counterions are shown as spheres. The solvent is omitted for clarity.

this finding is in agreement with experimental data⁴² and with Brownian dynamics simulations.⁴³ As demonstrated in Ref. 43, and as we proceed to show, the fact that $\langle R_g^2 \rangle_{\text{term}} > \langle R_g^2 \rangle_{\text{dend}}$ does *not* mean that beads of the terminal generation shell are localized near the dendrimer's periphery.

To clarify the role of counterions, we calculated the mean-square radius of gyration $\langle R_g^2 \rangle_{\text{ions}}$ of the counterions, see Fig. 4 (top), that serves as a measure for the size of the counterion cloud around the dendrimer. It turns out that the ion cloud becomes smaller as the Bjerrum length increases. This decrease, however, is found to be monotonic. Furthermore, in Fig. 4 (bottom) we estimate the fraction of counterions condensed onto the dendrimer. For doing that we used a simple criterion, namely, we counted counterions which had dendrimer beads in their first coordination shells. As Fig. 4 shows, the number of condensed ions increases continuously with the strength of electrostatic interactions in the system.

The above suggests that there is a subtle interplay between two opposite effects upon increasing λ_B : (i) a growth in the strength of the *repulsive* electrostatic interactions between the charged terminal beads and (ii) a strengthening of condensation of counterions due to the *attractive* interactions between counterions and the oppositely charged dendrimer beads. The former leads to a swelling of the charged den-

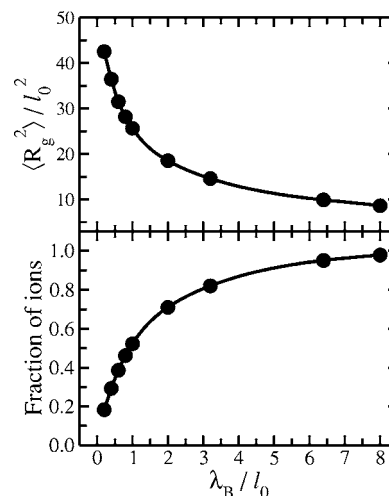


FIG. 4. Top: Average mean-square radius of gyration $\langle R_g^2 \rangle$ calculated for counterions with respect to the center of mass (c.m.) of the dendrimer. Bottom: Average fraction of counterions condensed onto the charged dendrimer as a function of the Bjerrum length λ_B . See text for the criterion used to identify condensed ions.

dimer and the latter screens positive charges of the terminal dendrimer generation giving rise to the shrinking of the dendrimer. The maximum of the dendrimer's size is found to be at $\lambda_B \approx 0.8l_0$ (i.e., at $\lambda_B \approx \sigma$), see Fig. 2. This corresponds to a swelling by $\sim 12.5\%$ with respect to the neutral case.

The condensation of counterions onto the dendrimer should be accompanied by a decrease in its hydration, which is characterized by the number of solvent molecules in the ion's first coordination shell. Indeed, that can be seen by computing the average coordination numbers of counterions with dendrimer's beads and with solvent molecules, see Fig. 5. The increase of the strength of electrostatic interactions in the system provokes a condensation of counterions and, correspondingly, leads to a loss of solvent molecules from the ions' first coordination (hydration) shell (Fig. 5).

C. Number density profiles

To analyze the locations of the dendrimer's beads, solvent molecules, and counterions in more detail, we calcu-

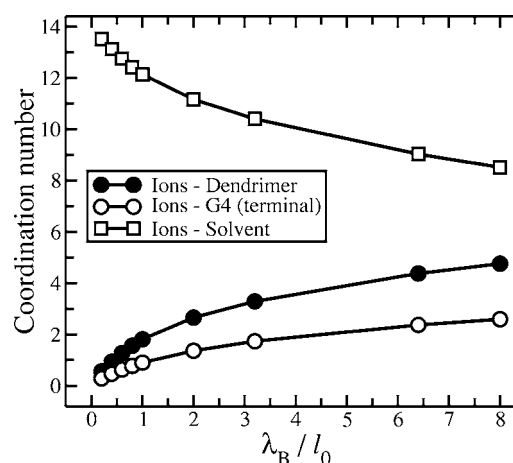


FIG. 5. Average coordination numbers of ions with the dendrimer's beads (solid circles), with the charged beads of the G4 shell (open circles), and with solvent beads (open squares) as a function of the Bjerrum length λ_B .

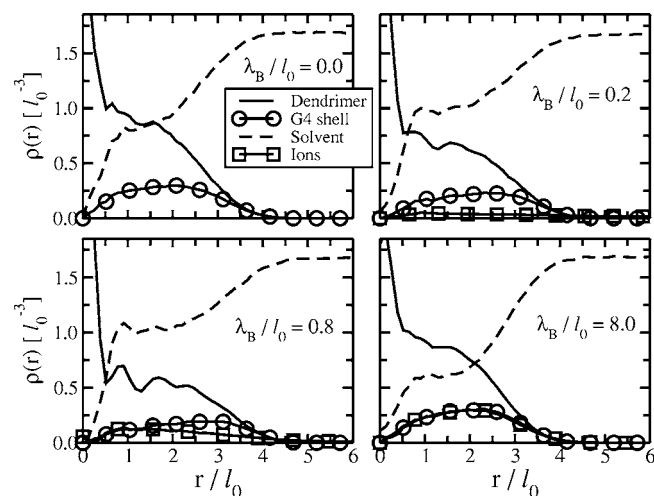


FIG. 6. Radial number densities $\rho(r)$ as a function of the distance r from the center of mass (c.m.) of the dendrimer for λ_B equal to 0.0, $0.2l_0$, $0.8l_0$, and $8.0l_0$.

lated component wise number density profiles $\rho(r)$ as a function of the radial distance r from the c.m. of the dendrimer, see Fig. 6 (Fig. 7 shows the corresponding radial bead distributions). For a neutral dendrimer the density profiles are in agreement with earlier molecular dynamics studies of dendrimers in an explicit solvent.²⁷ The overall number density of a dendrimer develops a plateau at $r > 0.5l_0$ from its c.m. The beads of the terminal shell are broadly distributed, implying a considerable degree of backfolding. The solvent molecules penetrate deeply into the dendrimer and their density profile has a plateau at $r > 0.5l_0$, see Fig. 6.

At small Bjerrum lengths ($\lambda_B \leq 0.8l_0$) the charged dendrimer swells and the density profile plateaus considerably with a simultaneous drop in the plateau's magnitude, see, e.g., Fig. 6 for $\lambda_B = 0.8l_0$. The charged beads of the terminal shell are redistributed towards the dendrimer's periphery making the interior of the dendrimer significantly more accessible for solvent and counterions.

Further increase in the Bjerrum length leads to a shrink-

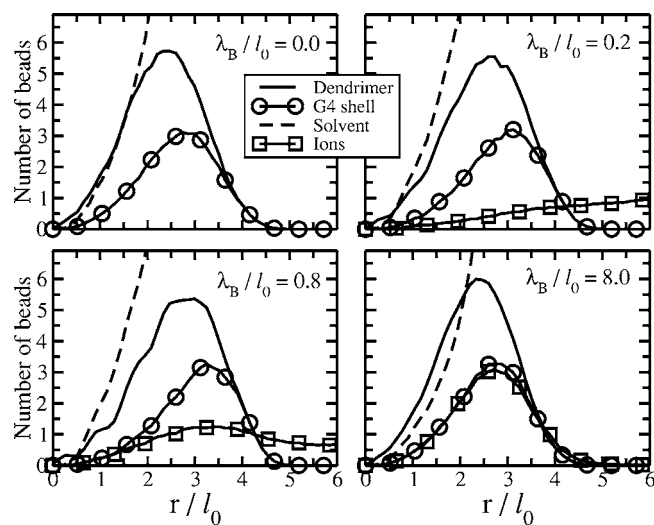


FIG. 7. The number of beads (corresponding to the number densities in Fig. 6) as a function of the distance r from the c.m. of the dendrimer.

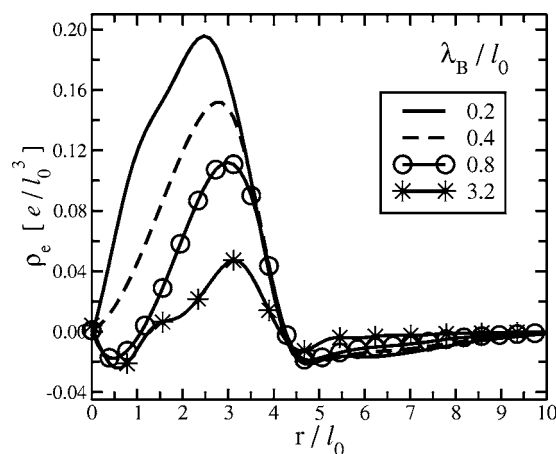


FIG. 8. Radial charge densities $\rho_e(r)$ as a function of the radial distance r from the c.m. of a dendrimer for λ_B equal to $0.2l_0$ (solid line), $0.4l_0$ (dashed line), $0.8l_0$ (solid line with circles), and $3.2l_0$ (solid line with stars). To reduce the noise in the data, the charge densities shown here were first fitted to splines (Ref. 44).

age since counterion condensation starts to dominate. Therefore, the dendrimer's density profile changes towards a similar profile as observed at small λ_B with one important exception: The amount of condensed ions increases considerably, and their density profiles overlap more and more with the density profiles of the charged terminal beads of the dendrimer (up to almost complete coincidence of the profiles in the case of extremely large Bjerrum lengths, see Fig. 6 for $\lambda_B = 8.0l_0$). This shrinkage is accompanied by a reduction of voids in the dendrimer's interior leading to the squeezing of solvent molecules out of the dendrimer, see Figs. 6 and 7.

D. Charge density profiles

Next, we take a look at the screening of the dendrimer's charges by counterions. In Fig. 8 we plot the charge density profiles $\rho_e(r)$ for the whole system as a function of the radial distance r from the c.m. of the dendrimer. We recall that since our solvent is nonpolar, the charge densities $\rho_e(r)$ are defined only by the interplay between the positively charged terminal beads and the negatively charged counterions. Figure 8 clearly demonstrates screening: The height of the positive $\rho_e(r)$ peaks drops drastically with increasing Bjerrum length as compared with the $\rho_e(r)$ peak for $\lambda_B = 0.2l_0$ when the counterion condensation has just started.

While the main peaks of all $\rho_e(r)$ curves are located in the domain of the positive charges, starting with $\lambda_B = 0.6l_0$, one observes small minima close to the c.m. of the dendrimer where $\rho_e(r)$ becomes negative, see Fig. 8. We address these minima to the fact that some of condensed counterions can be localized deep in the dendrimer's interior rather than beside charged terminal beads giving rise to an excess of negative charges close to the dendrimer's center of mass, see Figs. 6 and 7. In turn, on the right of $\rho_e(r)$ peaks we see another region where the overall charge of the system is also negative. This region of negative charge, being associated with "unbound" counterions in bulk solvent, becomes smaller with λ_B and eventually disappears at large Bjerrum lengths.

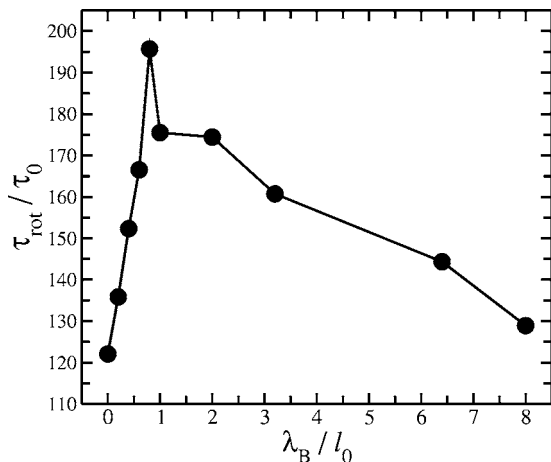


FIG. 9. Characteristic relaxation time τ_{rot} related to the dendrimer's reorientational dynamics as extracted from the autocorrelation function of the unit vector pointing from the c.m. of the dendrimer to the beads of its terminal G4 generation shell. Error bars are of the order of the symbol size.

IV. DYNAMIC PROPERTIES

The molecular dynamics simulation technique provides an access to the dynamic properties, and next we discuss the dynamics of charged dendrimers in a salt-free solution.

A. Global reorientational dynamics

First, we consider the relaxation of vectors pointing from the c.m. of the dendrimer to the beads of a given generation shell.^{18,27,45} If the terminal (G4) generation shell is considered, the corresponding autocorrelation function (ACF) of “c.m.-G4” vector can be employed to analyze the global reorientational behavior of the whole dendrimer.²⁷ It is, however, necessary to bear in mind that there is no reason for the beads of the last generation to be located at the dendrimer's periphery.

To characterize the dendrimer's rotation, we calculated the ACF of the *unit* vector directed along the c.m.-G4 vector. The corresponding relaxation times τ_{rot} were extracted from the autocorrelation functions as follows. First, it was ascertained that the ACF can be characterized by a single relaxation time, namely, that the time dependence of the natural logarithm of the ACF was roughly linear. Then, the relaxation time was defined as the time of the ACF decay by a factor of e .

Figure 9 shows that the global reorientational motion of the charged dendrimer depends nonmonotonically on the Bjerrum length. Such a behavior resembles the λ_B dependence of $\langle R_g^2 \rangle$ as was seen earlier in Fig. 2. This is expected since it is reasonable to assume that the global reorientational dynamics is controlled by the dendrimer's size: Larger size requires more time for reorientation.

B. Local dynamics of bonds and dendrimer's core

As seen in Fig. 9, the global reorientational dynamics is determined by rather long characteristic times up to $\sim 200\tau_0$. The local orientational motions are characterized by much shorter times. As an example, we consider here the reorientation dynamics of the bond vectors $\mathbf{b}_i(t)$. In Fig. 10 we plot

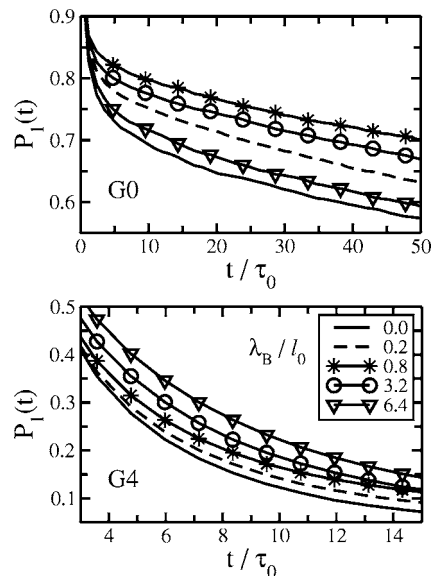


FIG. 10. Time evolution of the normalized autocorrelation function $P_1(t) = \langle \mathbf{b}_i(0)\mathbf{b}_i(t) \rangle$ of bond vectors $\mathbf{b}_i(t)$ of the innermost (top) and the outermost (bottom) shells. The legend shows the different Bjerrum lengths used.

the time evolution of the corresponding autocorrelation function $P_1(t) = \langle \mathbf{b}_i(0)\mathbf{b}_i(t) \rangle$ for the innermost (G0) and the outermost (G4) shells. We note that the relaxation of $P_1(t)$ cannot be characterized by a single relaxation time. Therefore, we focus here on the time behavior of $P_1(t)$ rather than on characteristic times.

The reorientation of a bond slows down with the size of the dendrimer, see Fig. 10 (top). Such a behavior is found to hold for all inner generation shells from G1 to G3 (data not shown). Remarkably, the above nonmonotonic (notice the order of the curves) dependence on λ_B in Fig. 10 (top) breaks down for $P_1(t)$ of the terminal (outermost) generation shell as it is seen in Fig. 10 (bottom). This feature can be linked to the condensation of counterions which plays a dominant role at $\lambda_B > 0.8l_0$ and, therefore, can hinder the reorientation of bonds of the terminal G4 shell.

The local reorientation dynamics of dendrimer bonds can also be characterized by the autocorrelation function $P_2(t) = (3/2)(\langle \mathbf{b}_i(0)\mathbf{b}_i(t) \rangle^2 - 1/3)$. It turns out that the simple relation $P_2(t) = P_1^3(t)$ holds for all bonds in agreement with the previous simulation studies.¹⁸

Last, we focus on the relaxation of the vector pointing from the dendrimer's center of mass to its core (“c.m.-core” vector).¹⁸ The core and the c.m. are typically found to be very close to each other. However, they do not exactly coincide and the relaxation of the corresponding c.m.-core vector is characterized by small (but finite) relaxation times.

In Fig. 11 we plot the corresponding characteristic relaxation times τ_{core} , which were determined from corresponding autocorrelation functions in the same manner as described in Sec. IV A. As argued above, the relaxation times turn out to be very small, just a few τ_0 . The λ_B dependence of the τ_{core} resembles the behavior of the $\langle R_g^2 \rangle$ curve in Fig. 2, i.e., increase in the dendrimer size speeds up the relaxation of the c.m.-core vector and vice versa. This effect can be explained in terms of the mobility of a dendrimer core: Larger den-

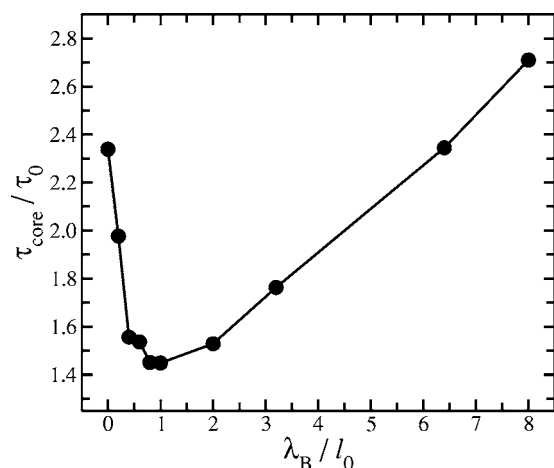


FIG. 11. The characteristic relaxation time τ_{core} for a vector pointing from the c.m. of a dendrimer to its core as a function of the Bjerrum length λ_B . Error bars are of the order of the symbol size.

drimers are characterized by smaller densities of their interior (see Fig. 6) and, therefore, by more mobile cores which relax faster.

V. DISCUSSION AND CONCLUSIONS

We have performed a systematic molecular dynamics study of generic cationic dendrimers solvated in explicit solvent in the presence of explicit counterions. The main goal was to understand to what degree the structural and dynamic properties of charged dendrimers are sensitive to the strength of electrostatic interactions, and what is the role of counterions.

We found an intriguing interplay between the *repulsive* interactions of the dendrimer's charged terminal beads and their *attractive* interactions with oppositely charged counterions. Depending on the type of dominant interactions, one observes swelling or shrinking of the molecule as the strength of the electrostatic interactions is increased. In other words, the size of a charged dendrimer depends *nonmonotonically* on the Bjerrum length λ_B as shown in Fig. 2. Most of the dendrimer's structural and dynamic characteristics considered in this study were found to follow this pattern.

For small Bjerrum lengths a charged dendrimer swells with λ_B and its size reaches maximum at $\lambda_B=0.8l_0$. At larger Bjerrum lengths the condensation of counterions dominates and the dendrimer shrinks. The counterion condensation is often discussed in the framework of the Manning theory,⁴⁶ which predicts the condensation to occur when $\lambda_B/a \geq 1$ where a is the distance between charges along the polymer backbone. However, Manning's criterion is not applicable in our case. Manning's theory is formulated for linear polyelectrolytes and not for spherical-like branched objects such as dendrimers. Second, the charged dendrimer considered in our study has only its terminal beads charged, making the meaning of the parameter a uncertain. The counterion condensation, the effects of valence, charging, and the size and shape of the dendrimer could more appropriately be studied using the method of Patra *et al.*⁴⁷ who studied the charging of spherical three dimensional objects under different condi-

tions. A detailed study of the above factors is, however, beyond the current work and will be addressed in a future publication.

The Bjerrum length $\lambda_B=\sigma$ corresponds to the position of the $\langle R_g^2 \rangle$ peak, see Fig. 2, and, therefore, separates swelling and shrinking regimes. Remarkably, on the left-hand side of the peak, the separation between charges *always* exceeds the Bjerrum length because the beads cannot get closer than σ and $\lambda_B < \sigma$. On the other hand, the counterion condensation is rather weak in this λ_B domain. Therefore, one can expect the Debye-Hückel approximation to be valid at around $\lambda_B \leq \sigma$ and to break down at larger Bjerrum lengths.

It is instructive to relate the dendrimer bond length l_0 (and, correspondingly, the average dendrimer size R_g and the Bjerrum length λ_B) to the characteristic length scales typical for real dendrimers in aqueous solutions. The value of 17.1 \AA is available from small angle x-ray scattering experiments⁴⁸ for the average radius of gyration R_g of a PAMAM dendrimer of the fourth generation. A very recent MD study²¹ reported $R_g=16.78 \pm 0.15 \text{ \AA}$ for a nonprotonated PAMAM dendrimer in explicit water. In another study, Lee *et al.*²⁰ reported $R_g=14.8 \pm 0.1 \text{ \AA}$, that was obtained from MD studies of PAMAM dendrimers without a solvent ($R_g=14.50 \pm 0.28 \text{ \AA}$ in Ref. 21 was obtained under the same conditions). Assuming that dendrimer swells on about 15% in water,²¹ the results of Lee *et al.*²⁰ seem to be in accord with other studies. We took $R_g \approx 17 \text{ \AA}$ for our parametrization. For a neutral dendrimer we have $R_g \approx 2.54l_0$, see Fig. 2, such that $l_0 \approx 6.7 \text{ \AA}$.

Thus, the critical Bjerrum length corresponding to the dendrimer's maximal size can be estimated to be 5.4 \AA . In turn, the Bjerrum length in water at 300 K is about 7.1 \AA (or $\sim 1.3l_0$), i.e., it exceeds the critical value. In practice, since the $\langle R_g^2 \rangle$ peak is not very sharp, the value of $\langle R_g^2 \rangle$ for a dendrimer in *water*, being located next to the peak, is rather close to the maximum of $\langle R_g^2 \rangle$, see Fig. 2. Taking also into account the uncertainty in defining the value of l_0 , one can conclude that counterion condensation will not affect significantly PAMAM dendrimers in water under physiological conditions.

To summarize, we demonstrated that including explicit counterions can have a dramatic effect on the structure and dynamics of charged dendrimers, and under certain conditions they cannot be treated implicitly. Therefore, simplified approaches, such as the well-known Debye-Hückel approximation, have to be applied with great care. Given that the most exciting applications of protonated dendrimers are related to drug and gene delivery, it would be interesting to clarify the role of counterions in the complexation of charged dendrimers with linear polyelectrolytes bearing opposite charges.^{49,50} This problem is addressed in our ongoing studies.

ACKNOWLEDGMENTS

Fruitful discussions with Dr. Alexey V. Lyulin and Professor Anatoly A. Darinskii are gratefully acknowledged. This work has been supported by the Academy of Finland through its Center of Excellence Program to two of the au-

thors (A.A.G. and I.V.) and through Grant Nos. 202598 (A.A.G.), 80246 (I.V.), 00119 (M.K.), 54113 (M.K.), and 211579 (S.V.L.) and by the Russian Foundation of Basic Research through Grant Nos. 05-03-32332 (A.A.G.) and 05-03-32450-a (S.V.L.). One of the authors (S.V.L.) acknowledges the support of the Government of St. Petersburg, Russia (Grant No. PD 05-1.3-101) and of the NWO (Grant 047.019.001) and another author (M.K.) the support from the Emil Aaltonen Foundation (Finland). The simulations were performed on the HorseShoe (DCSC) supercluster at the University of Southern Denmark.

- ¹J. M. J. Fréchet, *Science* **263**, 1710 (1994).
- ²R. F. Service, *Science* **267**, 458 (1995).
- ³I. Jääskeläinen, S. Peltola, P. Honkakoski, J. Mönkkönen, and A. Urtti, *Eur. J. Pharm. Sci.* **10**, 187 (2000).
- ⁴U. Boas and P. M. H. Heegaard, *Chem. Soc. Rev.* **33**, 43 (2003).
- ⁵M. Ozkan, *Drug Discovery Today* **9**, 1065 (2004).
- ⁶R. C. van Duijvenbode, M. Borkovec, and G. J. M. Koper, *Polymer* **39**, 2657 (1998).
- ⁷J. F. KukowskaLatallo, A. U. Bielinska, J. Johnson, R. Spindler, D. A. Tomalia, and J. R. Baker, *Proc. Natl. Acad. Sci. U.S.A.* **93**, 4897 (1996).
- ⁸A. Bielinska, J. F. KukowskaLatallo, J. Johnson, D. A. Tomalia, and J. R. Baker, *Nucleic Acids Res.* **24**, 2176 (1996).
- ⁹M. J. Liu and J. M. J. Fréchet, *Pharm. Sci. Tech. Today* **2**, 393 (1999).
- ¹⁰R. Esfand and D. A. Tomalia, *Drug Discovery Today* **6**, 427 (2001).
- ¹¹M. J. Cloninger, *Curr. Opin. Chem. Biol.* **6**, 742 (2002).
- ¹²N. D. Sonawane, F. C. Szoka, Jr., and A. S. Verkman, *J. Biol. Chem.* **45**, 44826 (2003).
- ¹³E. R. Gillies and J. M. J. Fréchet, *Drug Discovery Today* **10**, 35 (2005).
- ¹⁴M. Ballauff and C. N. Likos, *Angew. Chem., Int. Ed.* **43**, 2998 (2004).
- ¹⁵A. A. Gurtovenko and A. Blumen, *Adv. Polym. Sci.* **182**, 171 (2005).
- ¹⁶P. Welch and M. Muthukumar, *Macromolecules* **31**, 5892 (1998).
- ¹⁷S. V. Lyulin, L. J. Evers, P. van der Schoot, A. A. Darinskii, A. V. Lyulin, and M. A. J. Michels, *Macromolecules* **37**, 3049 (2004).
- ¹⁸S. V. Lyulin, A. A. Darinskii, A. V. Lyulin, and M. A. J. Michels, *Macromolecules* **37**, 4676 (2004).
- ¹⁹T. Terao and T. Nakayama, *Macromolecules* **37**, 4686 (2004).
- ²⁰I. Lee, B. D. Athey, A. W. Wetzel, W. Meixner, and J. R. Baker, *Macromolecules* **35**, 4510 (2002).
- ²¹P. K. Maiti, T. Cagin, S. T. Lin, and W. A. Goddard III, *Macromolecules* **38**, 979 (2005).
- ²²S.-T. Lin, P. K. Maiti, and W. A. Goddard III, *J. Phys. Chem. B* **109**, 8663 (2005).
- ²³M. J. Stevens and K. Kremer, *J. Chem. Phys.* **103**, 1669 (1995).
- ²⁴C. Holm, K. Kremer, M. Deserno, and H. J. Limbach, in the *Proceedings of the NIC Symposium 2001*, edited by H. Rollnik and D. Wolf (NIC, Jülich, 2001), Vol. 9, pp. 385–395.
- ²⁵S. Liu and M. Muthukumar, *J. Chem. Phys.* **116**, 9975 (2002).
- ²⁶D. E. Galperin, V. A. Ivanov, M. A. Mazo, and A. R. Khokhlov, *Polym. Sci., Ser. A Ser. B* **47**, 61 (2005).
- ²⁷K. Karatasos, D. B. Adolf, and G. R. Davies, *J. Chem. Phys.* **115**, 5310 (2001).
- ²⁸T. Darden, D. York, and L. Pedersen, *J. Chem. Phys.* **98**, 10089 (1993).
- ²⁹U. Essman, L. Perera, M. L. Berkowitz, H. L. T. Darden, and L. G. Pedersen, *J. Chem. Phys.* **103**, 8577 (1995).
- ³⁰M. Patra, M. Karttunen, M. T. Hyvönen, E. Falck, P. Lindqvist, and I. Vattulainen, *Biophys. J.* **84**, 3636 (2003).
- ³¹M. Patra, M. Karttunen, M. T. Hyvönen, E. Falck, and I. Vattulainen, *J. Phys. Chem. B* **108**, 4485 (2004).
- ³²M. Murat and G. S. Grest, *Macromolecules* **29**, 1278 (1996).
- ³³B. Dünweg and K. Kremer, *J. Chem. Phys.* **99**, 6983 (1993).
- ³⁴R. Chang and A. Yethiraj, *J. Chem. Phys.* **118**, 6634 (2003).
- ³⁵H. J. C. Berendsen, J. P. M. Postma, W. F. van Gunsteren, A. DiNola, and J. R. Haak, *J. Chem. Phys.* **81**, 3684 (1984).
- ³⁶J. P. Ryckaert, G. Ciccotti, and H. J. C. Berendsen, *J. Comput. Phys.* **23**, 327 (1977).
- ³⁷H. J. C. Berendsen, D. van der Spoel, and R. van Drunen, *Comput. Phys. Commun.* **91**, 43 (1995).
- ³⁸E. Lindahl, B. Hess, and D. van der Spoel, *J. Mol. Model.* **7**, 306 (2001).
- ³⁹R. A. Böckmann, A. Hac, T. Heimburg, and H. Grubmüller, *Biophys. J.* **85**, 1647 (2003).
- ⁴⁰A. A. Gurtovenko, *J. Chem. Phys.* **122**, 244902 (2005).
- ⁴¹A. A. Gurtovenko, M. Miettinen, M. Karttunen, and I. Vattulainen, *J. Phys. Chem. B* **109**, 21126 (2005).
- ⁴²A. Topp, B. J. Bauer, J. W. Klimash, R. Spindler, D. A. Tomalia, and E. J. Amis, *Macromolecules* **32**, 7226 (1999).
- ⁴³A. V. Lyulin, G. R. Davies, and D. B. Adolf, *Macromolecules* **33**, 6899 (2000).
- ⁴⁴B. J. Thijssse, M. A. Hollanders, and J. Hendrikse, *Comput. Phys.* **12**, 393 (1998).
- ⁴⁵C. Cai and Z. Y. Chen, *Macromolecules* **30**, 5104 (1997).
- ⁴⁶G. S. Manning, *Q. Rev. Biophys.* **11**, 179 (1978).
- ⁴⁷M. Patra, M. Patriarca, and M. Karttunen, *Phys. Rev. E* **67**, 031402 (2003).
- ⁴⁸T. J. Prosa, B. J. Bauer, E. J. Amis, D. A. Tomalia, and R. Scherrenberg, *J. Polym. Sci., Part B: Polym. Phys.* **35**, 2913 (1997).
- ⁴⁹P. Welch and M. Muthukumar, *Macromolecules* **33**, 6159 (2000).
- ⁵⁰S. V. Lyulin, A. A. Darinskii, and A. V. Lyulin, *Macromolecules* **38**, 3990 (2005).